The Effect of Ambient Ageing on the Corrosion Protective Properties of a Lithium-Based Conversion Layer

Li, Ziyu; Homborg, Axel; Gonzalez-Garcia, Yaiza; Visser, Peter; Soleimani, Mohammad; Mol, Arjan

DOI
10.1149/1945-7111/acc1a6

Publication date
2023

Document Version
Final published version

Published in
Journal of the Electrochemical Society

The Effect of Ambient Ageing on the Corrosion Protective Properties of a Lithium-Based Conversion Layer

Journal of The Electrochemical Society, 2023 **170** 031504
1945-7111/2023/170(3)/031504/11/$40.00 © 2023 The Electrochemical Society ("ECS"). Published on behalf of ECS by IOP Publishing Limited

The Effect of Ambient Ageing on the Corrosion Protective Properties of a Lithium-Based Conversion Layer

Ziyu Li,[1] Axel Homborg,[1,2] Yaiza Gonzalez-Garcia,[1] Peter Visser,[3] Mohammad Soleimani,[1] and Arjan Mol[1,z]

[1]*Delft University of Technology, Department of Materials Science and Engineering, Mekelweg 2, 2628CD Delft, The Netherlands*
[2]*Netherlands Defence Academy, Het Nieuwe Diep 8, 1781 AC Den Helder, The Netherlands*
[3]*AkzoNobel, Rijksstraatweg 31, 2171 AJ, Sassenheim, The Netherlands*

The influence of ageing under ambient conditions on the corrosion protective behaviour of a lithium-based conversion layer on AA2024-T3 is studied in this work. Conversion layers aged at ambient conditions for relatively short times (0 h and 4 h), show an initial high degree of corrosion inhibition but a much lower protectiveness after the inhibition stage terminates. Conversion layers with relatively long ageing times (24 h and 72 h) show a rather stable corrosion resistance which is higher than that of short-time aged samples. It is hypothesized that the freshly-formed conversion layer has trapped a certain amount of lithium ions and water molecules, leading to ongoing and heterogeneous growth of the conversion layer with time under ambient indoor conditions. Moreover, conversion layers with short ageing times show early-stage active corrosion protection by lithium-ion release.
 [DOI: 10.1149/1945-7111/acc1a6]

Manuscript submitted January 17, 2023; revised manuscript received March 3, 2023. Published March 17, 2023. *This paper is part of the JES Focus Issue on Critical Factors in Localized Corrosion in Honor of Gerald Frankel.*

Supplementary material for this article is available online

Aluminium alloys are widely applied in the aerospace industry for their favourable workability and high strength-to-weight ratio due to the presence of strengthening alloying elements like copper or zinc.[1–4] However, these alloying elements usually contribute to the generation of a complex and heterogeneous microstructure, leading to the increased susceptibility of localised corrosion.[5–7] Therefore, most aluminium alloys cannot be practically applied without adequate surface treatments.[8]

Numerous surface treatment techniques have been developed to provide effective surface protection for aluminium alloys, such as organic coatings,[9,10] anodizing,[11–13] sol-gel synthesis[14–16] and chemical conversion films.[17–19] Chemical conversion coatings are often favoured because of their easy preparation process and cost-effectiveness. Conversion treatments can change the metallic interface from an active to a passive state and conversion films can also be used as base layers to strengthen the adhesion force of the organic coatings.[8,19] Chromate conversion coatings (CCCs), most notably hexavalent chromium (Cr(VI)), have been employed in the protection of many aerospace aluminium alloys to suppress corrosion and to improve surface adhesion.[8,20,21] However, the European Regulation Registration, Evaluation, Authorization and restriction of Chemicals (REACH) announced a ban on Cr(VI) in 2013 due to its high toxicity and carcinogenicity.[22]

As a consequence, the replacement of chromate conversion coatings by novel eco-friendly conversion treatments has been strongly motivated. Among various alternatives, lithium salts have been introduced as a candidate to replace Cr(VI)-based chemistries due to their competitive price and potential protection efficiency.[23–26] Initially, it was reported that aluminium underwent inhibition when exposed to an alkaline electrolyte containing lithium ions.[23,24] Further studies revealed that lithium ions were readily intercalated into the aluminium hydroxide, stabilizing the corrosion products when the alloy surface was exposed to an aggressive alkaline environment.[25,26] Further studies from Buchheit et al.[27–29] revealed that the enhanced corrosion protection is caused by the formation of an Al-Li layered double hydroxide layer. This surface modification passed a 168-hour salt spray test. Another breakthrough in the application of lithium salts came from Visser et al. in 2010, when a polyurethane organic coating loaded with lithium salts was proven to provide effective corrosion inhibition by the formation of a protective conversion layer in coating defects during the neutral salt spray test (ASTM B-117).[30] The active and barrier protection properties of the lithium-based inhibitor coating technology have been well documented over the last years by a wide variety of electrochemical, microscopic and spectroscopic studies,[31–39] indicating that the application of lithium salts represents a promising strategy for the further replacement of Cr(VI)-containing protective coatings.

Compactness and integrity are important characteristics of the protective abilities of a conversion layer. However, freshly formed chromate-free conversion coatings usually are rich in defects or cracks due to dehydration.[40–46] The defect areas provide pathways for corrosive electrolyte ingress leading to a significant decrease of the corrosion protection performance of conversion layers.[41] Dehydration usually is inevitable since conversion coatings are formed in an aqueous environment, resulting in water entrapment within the coatings. Drying or ageing treatment will cause water evaporation and generate newly-formed defects due to the dehydration-driven shrinkage of the conversion layers.[41,43] However, the influence of an ageing treatment after conversion layer formation is reported to not always lead to decreasing corrosion protective properties. It was reported by Li et al. that trivalent chromium process (TCP) coatings underwent dehydration and condensed after ageing at elevated temperatures (⩽100 °C), accompanied by the generation of a low defect-density conversion layer.[40] Moreover, longer ageing at room temperature was reported to also enhance the corrosion resistance of the TCP coating by a factor 4, which was attributed to the formation of an aluminium oxide layer and increasing hydrophobicity of the conversion coating. On the other hand, other studies have reported a negative impact of ageing on corrosion protectiveness of TCP coatings.[42,43] This might be due to the different conversion treatment parameters and post-formation ageing conditions, which result in different physico-chemical and electrochemical properties. While prior studies show that lithium-based conversion layers show promise among chromate-free conversion coatings, the influence of post-formation ageing on its corrosion protectiveness has remained yet unknown.

In the present work, the influence of ageing duration under indoor ambient conditions on the protectiveness of lithium-based conversion layers was studied using Electrochemical noise (EN) and top-view and cross-sectional micrographs. Earlier work has shown that EN analysis can be a powerful technique to study the corrosion protective behaviour of the lithium-based conversion layer.[47] Top-

[z]E-mail: J.M.C.Mol@tudelft.nl

view and cross-sectional micrographs were obtained by focused ion beam-scanning electron microscopy (FIB-SEM) to distinguish layer morphology changes to the conversion layers upon ageing and upon re-immersion to a corrosive solution to underpin the differences in corrosion protective behaviour caused by ageing under ambient indoor conditions.

Experimental

Material and experimental set-up.—All working electrode material originated from a single commercial AA2024-T3 sheet provided by Goodfellow in 0.8 mm thickness. From this sheet, smaller rectangular specimens with a size of 8 mm × 18 mm and 20 mm × 20 mm were produced. The former was used for EN measurements and the latter were employed for immersion tests. Two specimens with a size of 8 mm × 18 mm were embedded in a commercial epoxy resin at a spacing of 2 mm after spraying a primer at four edges to avoid crevice corrosion. The EN control group consisted of embedded samples with a 5 mm spacing. All samples were ground up to grit 4000 SiC abrasive paper, gently cleaned with distilled water, dried by compressed air, and left in an ambient lab environment for 24 h before the start of the experiments. For samples with two identical panels, the electrical connection to external equipment was realized by two conductive copper tapes. For all samples, water-proof tape was used to cover the surfaces with a circular opening of either 10 mm or 15 mm in diameter to fix and limit the exposed area. The latter was only used for the pH measurement. The detailed setup of the electrochemical cell was described in our previous work.[47] Laboratory-grade chemicals used in this work were ordered from Sigma-Aldrich (St. Louis, MO, USA).

Sample preparation.—EN samples were covered by tape with a circular recess of 10 mm in diameter. 0.01 M NaCl and 0.01 M Li_2CO_3 (pH 10.9) solution was prepared to enable the formation of a lithium-based conversion layer and to mimic the local aqueous environment of a scribed area, which is consistent with previous work by the authors.[37,47] A 4 mm high electrolyte layer (0.321 ml) was established for experimental sample sets aiming to mimic the local liquid environment inside an artificial defect on an inhibitor-loaded organic coating.[48] For the control groups, 0.321 ml solution was added to the cell containing the samples at a 5 mm spacing and 1 ml solution was added into the cell, including the samples at a 2 mm spacing, to generate different lithium-based conversion layers. All experiments were performed under aerated conditions. Hydrogen bubbles generated during layer formation were gently removed every 10 min to form a relatively uniform lithium-based conversion layer. The exposure duration for coupons in 0.01 M NaCl and 0.01 M Li_2CO_3 solution was 14500 s (approximately 4 h). Later, the original electrolyte was removed, and the freshly formed conversion layers were gently rinsed using 0.01 M NaCl to remove superficially adsorbed lithium carbonate. Subsequently, samples were left in a lab environment at approximately 20 °C, 40% relative humidity for 0 h, 4 h, 24 h, and 72 h, respectively. Finally, samples were re-immersed in a 0.321 ml 0.01 M NaCl solution for 14500 s (approximately 4 h). EN current and potential responses were recorded simultaneously. The EN experimental procedure is shown in Fig. 1.

Single panels covered by the water-proof tape with a 10 mm diameter recess were used for SEM observation to avoid static charging of epoxy resin in the SEM. Here, the entire procedure (conversion layer growth, ageing and re-immersion) is identical to the one mentioned above for the EN measurements. Similarly, single panels covered by the tape with a 15 mm diameter recess were adopted for pH measurements since 0.321 ml is not suitable to obtain the minimum volume for a pH measurement during re-immersion. To establish a 4 mm electrolyte layer thickness for the immersion and re-immersion stages, 0.703 ml 0.01 M NaCl and 0.01 M Li_2CO_3, and 0.703 ml 0.01 M NaCl were added, respectively.

pH and ICP-OES measurement.—The pH values of the solution during re-immersion were measured by using a pH meter (Metrohm, 913 pH Meter). The dissolved lithium and aluminium ions from the lithium-based conversion layers were measured by Inductively Coupled Plasma-Optical Emission Spectroscopy (ICP-OES, Spectro, Arcos-EOP). Wavelengths relevant for Al detection are at 396.2 nm, 394.4 nm, and 167.0 nm, respectively while wavelength used for Li detection is at 670.8 nm. Detection limits for Al and Li are 0.01 mg/kg. The measurements were conducted at least in triplicate.

Focused ion beam-scanning electron microscopy (FIB-SEM) characterization.—To understand how ageing time altered the conversion layer, a series of cross-sectioning experiments were performed using a FIB-SEM (Helios G4 PFIB UXe, Thermo Fisher Scientific, USA) equipped with a xenon plasma focused ion beam (PFIB), operating at optimum conditions of an accelerating voltage of 30 kV and a beam current of 1 nA. The cross-sectional and top-view SEM morphological characterizations were performed at 10 keV collecting emitted secondary electrons (SE) in ultra-high-resolution mode. The chemical composition of different regions was estimated using Energy Dispersive Spectroscopy (EDS). It is worth noting that, to avoid any possible damage to the lithium-based conversion layer depositing, a protective Pt or C overlay coating was intentionally omitted.

Electrochemical noise (EN) measurements.—A traditional three-electrode EN setup containing two identical working electrodes and an Ag/AgCl/Saturated KCl reference electrode was used in this study. Potential values presented in this work are with respect to this reference electrode unless mentioned differently. All EN measurements were performed under open circuit conditions. A Compactstat from Ivium Technologies was used to record current and potential signals simultaneously, serving as a zero-resistance ammeter (ZRA) and potentiometer. The Compactstat was placed inside a Faradaic cage to avoid interference from external electromagnetic sources. The sampling frequency was set at 20 Hz and a low-pass filter of 10 Hz was used to avoid aliasing. The EN data were processed using Matlab from MathWorks. All EN tests were performed at least in triplicate.

EN signal processing.—In an EN measurement between two nominally identical corroding electrodes, these two electrodes are likely to behave non-stationary.[49] This causes an increasing asymmetry between these two electrodes.[50,51] In the EN current noise, the DC component does not contain information related to the electrochemical reactions occurring on the electrode surfaces other than the above-mentioned asymmetry. If this DC drift is not effectively removed, usually the relatively large amounts of energy present at the associated lower timescales may dominate over more useful, higher-frequency information during the data processing. Various methods can be used for DC drift removal, like moving average, polynomial and linear trend removal, wavelet analysis and empirical mode decomposition.[52,53] In this work, an eight-level discrete wavelet transform (DWT) with a Daubechies 4 wavelet was adopted due to its effective DC drift removal capacity while retaining sufficient useful corrosion information in the data.[50,51] This method has already proven to be effective in our previous work.[47] One application of EN in the time domain is to determine the variation in barrier properties of the lithium-based conversion layer over the course of the measurement by the noise resistance. It has been reported that the noise resistance is comparable to the near-DC polarization resistance.[54,55] Noise resistance is calculated as the ratio between the standard deviations of potential and current, after DC drift removal, within a user-defined time window. In the time-frequency domain, an energy distribution plot (EDP) was adopted to analyse the dominant timescales in an EN signal, and to study the relative contribution of reactions within specific frequency ranges.[56] The time scales shown in an EDP range from relatively short,

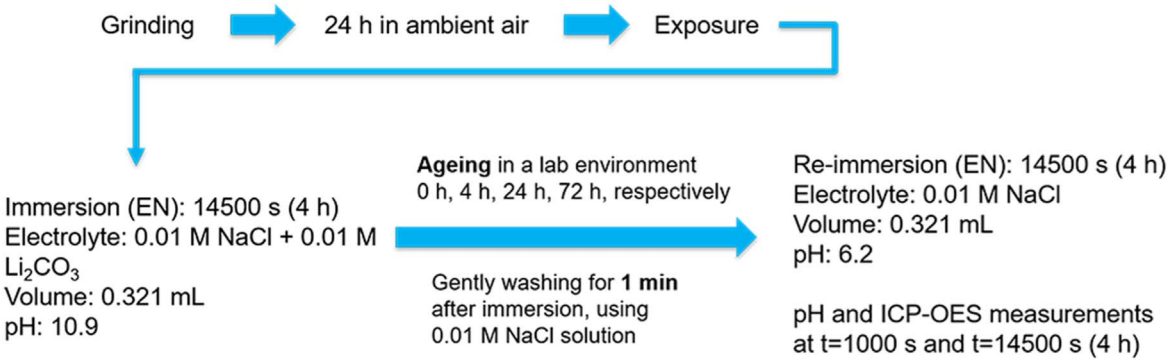

Figure 1. Sequence diagram of the experimental procedure for the EN, pH and ICP-OES measurements.

medium to long and correspond to activation-, mixed-, and diffusion-controlled processes, respectively.[52] The number of time scales is user-defined. It is generally accepted that an eight-level decomposition is sufficient to characterize corrosion characteristics.[57] Besides DWT, the continuous wavelet transform (CWT) spectrum was applied to extract time-frequency information using an analytic Morlet wavelet. For the CWT procedure, the signal is matched to a series of compressed or stretched variants of a wavelet. The duration of the wavelet corresponds to a specific frequency range. The CWT spectrum reveals the energy distribution of the EN signal over time and frequency simultaneously.

Results and Discussion

Corrosion resistance of the conversion layers.—Figure 2 shows EN current and potential signals recorded for the conversion layers during the re-immersion exposure for different ageing times. It is clear that for samples with 0 h (Figs. 2a and 4h (Fig. 2b) ageing, the potential signals show an initial drop and then a gradual increase, accompanied by relatively smooth current signals. At a later stage, an exposure stage including a relatively large number of transients in the signals follows. After 0 h ageing, this transition is accompanied by an instantaneous drop of the potential values and a very sharp increase of the absolute current values. The potential signal of the 0 h aged sample has a larger potential drop (minimum value close to −1000 mV) as compared to that of the 4 h aged coupon (minimum value close to −700 mV). In addition, the transition to the exposure stage also occurs at a later stage on the 0 h aged sample. In our previous work, the 0 h ageing data during re-immersion in 0.01 M NaCl solution was also analysed.[47] The large potential drop at the beginning can be attributed to the release of trapped lithium carbonate ions inside the previously formed conversion layer, which provides an extra active inhibition effect.[47] This effect will be discussed in detail later. For samples with 24 h (Fig. 2c) and 72 h (Fig. 2d) ageing, the initial potential drop is nearly absent, and the corrosion process starts as from the early-stage exposure to the NaCl electrolyte. The smooth potential and current signals in Figs. 2a and 2b are similar to the EN signals when AA2024-T3 was exposed to the lithium carbonate containing solution.[47] The authors designate this period as the inhibition stage, and the following period containing large amounts of transients as the corrosion stage. The corrosion stage occurs earlier for samples having undergone longer ageing times. It is therefore evident that the ageing treatment has a significant impact on the electrochemical properties and related corrosion protection provided by the lithium-based conversion layer.

For the purpose of investigating the barrier properties of the lithium-based conversion layer with different ageing times, the noise resistance is calculated. The results are presented in Fig. 3.

The horizontal black dashed lines represent the average value of the noise resistance after the potential signals reach a relatively stable value. The approximate start of this stage is indicated by a

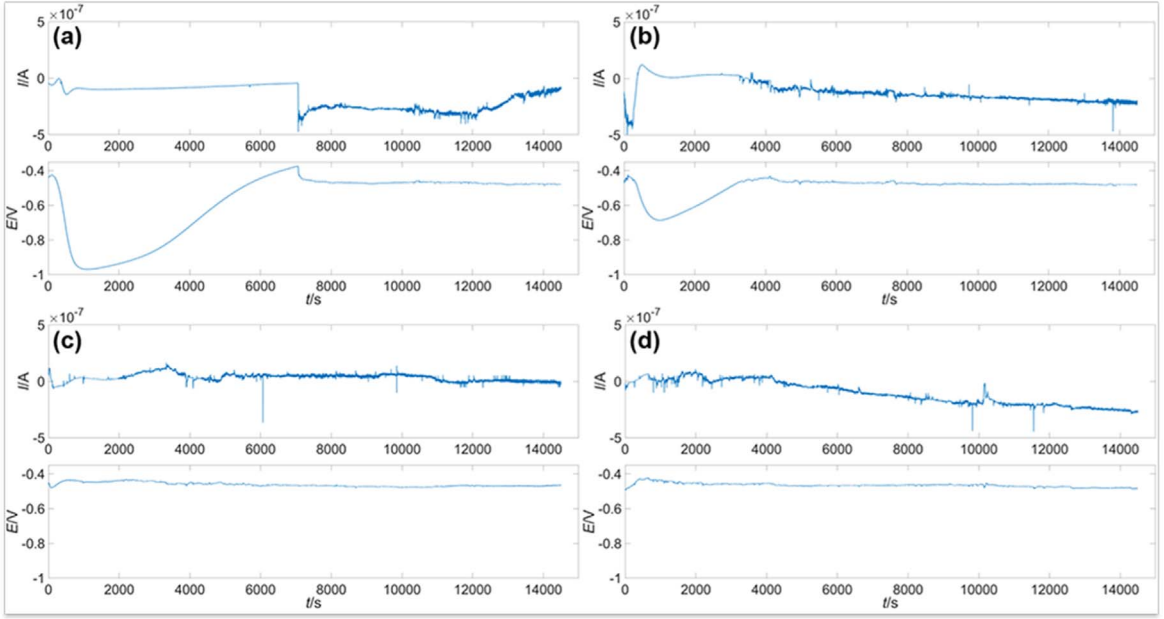

Figure 2. EN current (top) and potential (bottom) signals for AA2024-T3 initially treated in 0.01 M NaCl and 0.01 M Li_2CO_3 solution for 14500 s (approximately 4 h), and then exposed in 0.01 M NaCl after ambient ageing for (a) 0 h, (b) 4 h, (c) 24 h, and (d) 72 h.

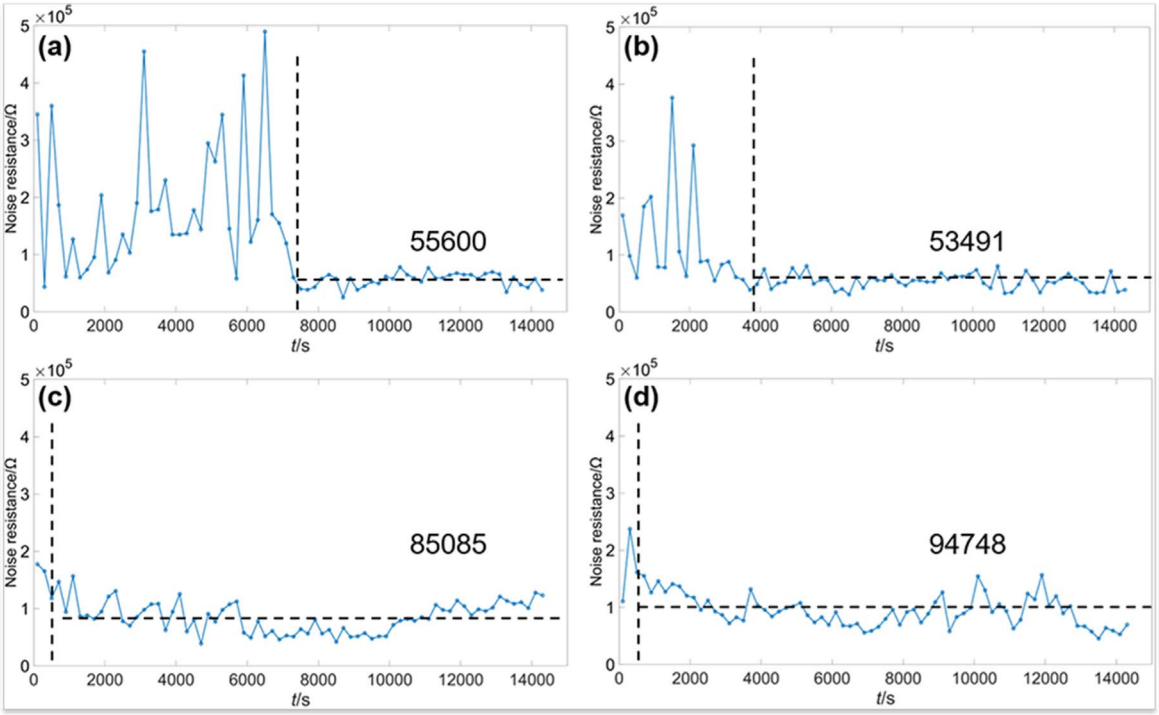

Figure 3. Noise resistance calculated for AA2024-T3 initially exposed in 0.01 M NaCl and 0.01 M Li_2CO_3 solution for 14500 s (approximately 4 h) and subsequently exposed in 0.01 M NaCl after ambient ageing for (a) 0 h, (b) 4 h, (c) 24 h, and (d) 72 h. The vertical dashed lines indicate the transition from inhibition to corrosion stage. The numbers (unit: Ω) shown in the figure indicate average noise resistance values in the corrosion stage.

vertical dashed line. In Figs. 3a and 3b, it is observed that the noise resistance presents a higher value with large oscillations before the sudden potential decrement. The 0h aged sample exhibits the largest noise resistance at the beginning, and the oscillations decrease significantly during the corrosion stage. In Figs. 3c and 3d, for the 24 h and 72 h aged samples, respectively, the noise resistance is relatively stable during the entire re-immersion. As for the average resistance value of samples with different ageing times, an interesting finding is that the noise resistance exhibits a very small drop for the 4h aged sample and then a notable improvement with longer ageing treatments. Therefore, long-time ageing treatments seem beneficial for enhancing the protective behaviour of the lithium-based conversion layer. To explain the phenomenon of improved corrosion protection capabilities for samples with longer ageing times in relation to the longer inhibited state for samples with shorter ageing times, compositional and morphological characterizations are required.

Dissolution behaviour of the conversion layers.—The noise resistance, with its relatively large oscillations during the inhibition stage, follows a similar trend as the lithium-based conversion layer's growth characteristics at later stages, with a competitive dissolution and growth in the solution containing lithium carbonate.[47,58,59] Therefore, this behaviour during the re-immersion tests may indicate the presence of residual lithium carbonate trapped in the conversion layer. This presence of lithium carbonate should be reflected in the pH, due to the alkaline nature of the carbonate ions,[48] and in the existence of dissolved lithium ions using ICP-OES measurements. Two time points (t = 1000 s, and t = 14500 s (approximately 4 h)) were selected to monitor the variation of pH and the released lithium and aluminium elements.

The pH variation of the conversion layers with different ageing treatments during re-immersion is shown in Fig. 4.

It is observed that all the samples experience a gradual pH increase during re-immersion and that the 0 h aged sample reaches the highest pH at two selected re-immersion times (t = 1000 s, t = 14500 s (approximately 4 h)). In addition, the pH increase upon re-immersion decreases with the ageing time. This observation implies that the release of alkalinizing species, such as carbonate ions, will gradually drop with extended ageing times. The dissolved amount of lithium and aluminium ions at t = 1000 s and t = 14500 s (approximately 4 h) is shown in Fig. 5. The dissolved lithium ions also present a decreasing trend with extended ageing times, corresponding well with the trend of the pH evolution, i.e. the carbonate ion release. The dissolved aluminium ions in the solution show a gradually rising trend with ageing time. This behaviour is caused by the earlier start of corrosion for longer-aged samples. Moreover, the adverse trends between dissolved lithium and aluminium ions confirm that the released lithium ions mainly

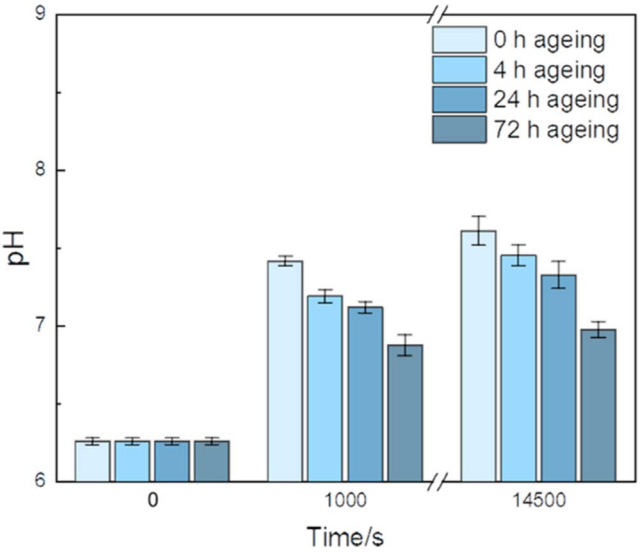

Figure 4. pH variation of the 0.01 M NaCl solution at selected re-immersion times for the differently aged samples.

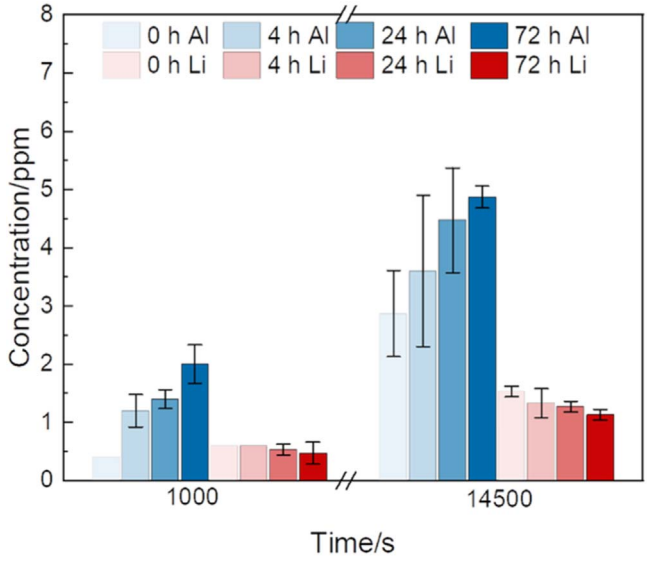

Figure 5. ICP-OES analysis of Al and Li ions released from the differently aged conversion layers. The standard deviation is calculated based on three data points.

originate from trapped lithium inside the conversion layer instead of the dissolution of the conversion layer itself. Consequently, the amount of mobile lithium ions within the conversion layer becomes smaller with extended ageing.

SEM characterisation of the conversion layers.—The top views of the lithium-based conversion layers dried under ambient indoor conditions for different ageing times are shown in Figs. 6a–6d, respectively.

A distinct morphological change with ageing time can be observed. Macroscopic cracks or crevices caused by dehydration are not observed for any of the differently aged samples, indicating that transients observed in Fig. 2 are likely to be attributed to the damage of the conversion layer during re-immersion. The morphology of the top columnar structure does not show an obvious growth or coarsening, but a large number of small particles appear on the top columnar layer for prolonged ageing. These particles show a similar porous structure as the top layer. In addition, both the size and coverage density of the particles increase with ageing time.

As reported previously, the lithium-based conversion layer formed on AA2024-T3 consists of a columnar top layer and an inner porous-to-dense layer.[37] Figure 7 shows the cross-sectional characterization of the conversion layers in the bare areas with different ageing treatments.

The conversion layer shown here consists of a well-developed outer columnar layer, but shows a less developed inner layer as compared to prior work,[37] predominantly caused by the relatively short conversion layer formation time in the present work. Furthermore, the cross-sectional micrographs confirm the top-view observation of the absence of macroscopic layer cracking or shrinkage from dehydration. Figure 8 shows the top-view and cross-sectional view of the conversion layer after re-immersion in 0.01 M NaCl solution for samples with 0 h, 4 h, 24 h, and 72 h ageing, respectively.

The conversion layer with 0 h ageing (Fig. 8a) presents the highest layer integrity as compared to the three other groups. Only few small pits are observed in the conversion layer, in line with the observation that the 0 h aged sample shows the longest inhibition stage: corrosion is only triggered at a later stage as compared to the other samples. Figures 8b–8d and 8b'–8d' indicate local corrosion, breakdown of the conversion layer and the presence of trenches around intermetallic phases for samples with 4 h, 24 h, and 72 h of ageing. Intermetallic phases surrounded by trenches are marked with a red dashed line. Trenches are a quite common morphological phenomenon during the corrosion stage of aluminium alloys,[7,60] even in case of the presence of cerium as inhibitor.[61] It can be inferred that the not fully-developed inner layer may provide local channels for corrosive ion ingress. Local conversion layer failure may occur due to the development of corrosion products at the substrate - conversion layer interface. The weak corrosion protection at the areas adjacent to intermetallic phases may be attributed to the lack of a protective dense inner layer covering the intermetallic phases,[36,37] more detailed information about the growth stage of the conversion layer at and around the areas of intermetallic phases can

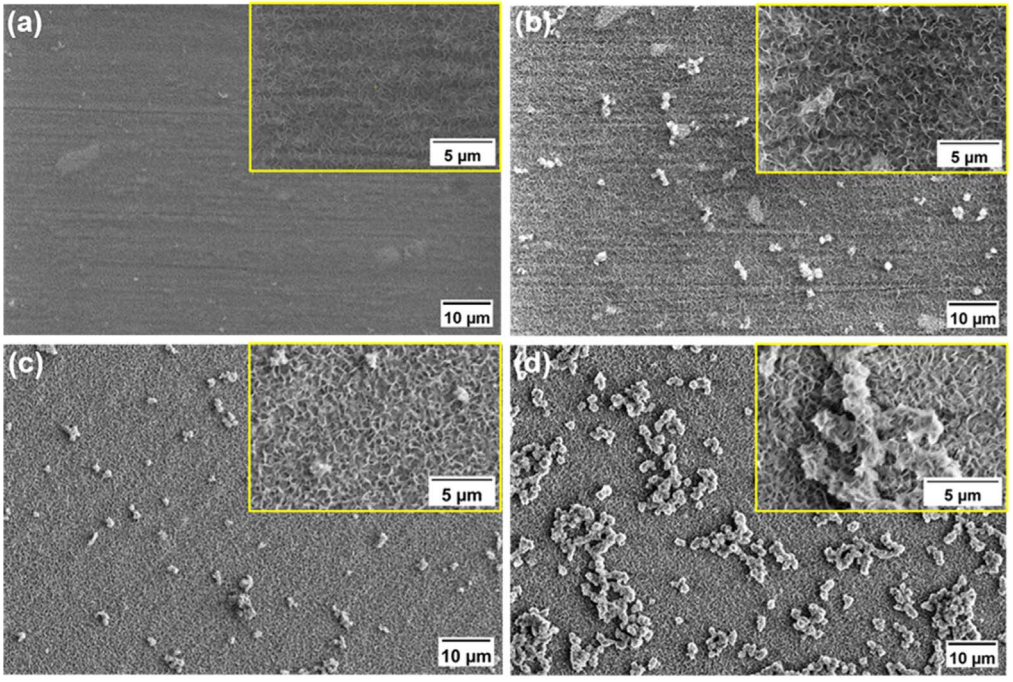

Figure 6. Top-view SEM images of the AA2024-T3 surface after immersion in an 0.01 M NaCl and 0.01 M Li_2CO_3 solution for 14500 s (approximately 4 h) and ambient ageing for (a) 0 h, (b) 4 h, (c) 24 h, and (d) 72 h.

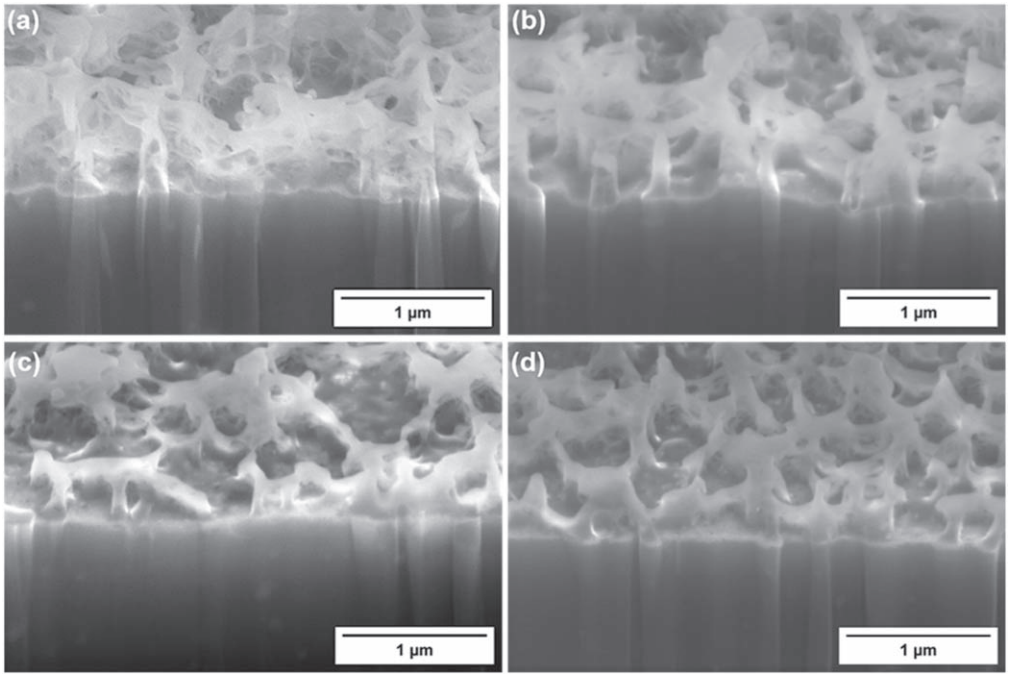

Figure 7. Cross-sectional observations of the conversion layer immersed in 0.01 M NaCl and 0.01 M Li_2CO_3 solution for 14500 s (approximately 4 h) after (a) 0 h, (b) 4 h, (c) 24 h, and (d) 72 h ageing, respectively.

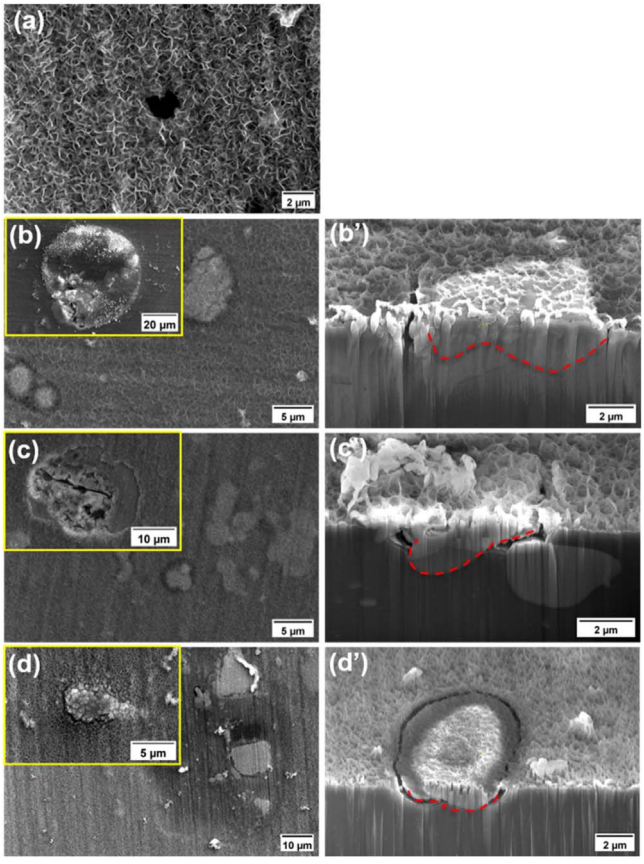

Figure 8. Top-view and cross-sectional observations of the conversion layer after immersion in 0.01 M NaCl and 0.01 M Li_2CO_3 solution for 14500 s (approximately 4 h), ageing for (a) 0 h, (b), (b') 4 h, (c), (c') 24 h and (d), (d') 72 h under ambient indoor conditions and re-immersion in a 0.01 M NaCl solution for 14500 s (approximately 4 h). Intermetallic contours are marked by the red dashed lines.

be found elsewhere.[37] Electrochemical impedance spectroscopy studies revealed that the dense inner layer normally dominates the corrosion protection provided by the entire conversion layer, whereas the top columnar layer is merely a minor contributor.[58]

A higher-magnification cross-sectional view of the conversion layer-covered particles is shown in Fig. 9. From the side view, the porous structure is more evident, and these aged particles seem to penetrate slightly into the aluminium matrix to form a more pronounced inner dense layer as shown in Fig. 9, in particular in Fig. 9c representing the longest aged sample, i.e. 72 h. The interface between the substrate and inner dense layer is each time indicated with a red dashed line.

The elemental compositions of the conversion layer and the particles on samples with different ageing times as measured by EDS are shown in Table I. As background information, an example of the selection of EDS points is shown in Fig. S1. The results show that the bare conversion layer and the ageing-formed particles share the same elemental constituents, which agrees with previous studies of the compositional characterization of the lithium-based conversion layer growing either on aluminium alloys, or inside the scratch of lithium-containing organic coatings.[36,62] Lithium and hydrogen are not listed due to the limitation of the EDS technique to detect such light elements.[36] In addition, ageing treatments from 4 h to 72 h under ambient indoor conditions do not significantly change the elemental compositions of the conversion layer or the aged particles. However, the particles do contain a higher content of oxygen and carbon and a lower percentage of aluminium. The higher content of carbon confirms the existence of trapped lithium carbonate ions, since carbonate is virtually the only carbon source for the growth of the conversion layer, whereas the percentage of carbon dioxide in the air is considered too low. The compositional differences are likely to originate from the different formation conditions. The bare conversion layer is formed in the electrolyte, whereas particles only appear after atmospheric exposure.

Time-frequency analysis of the EN current signals.—To further study the corrosion behaviour of the conversion layer during the corrosion stage, EN analysis was adopted to characterize the electrochemical properties in the time-frequency domain. The

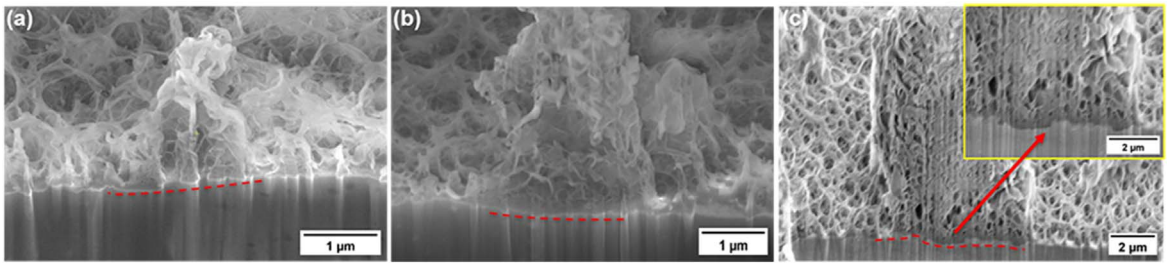

Figure 9. Cross-sectional observations of the particles grown on the conversion layer after immersion in a 0.01 M NaCl and 0.01 M Li_2CO_3 solution for 14500 s (approximately 4 h) and ageing for (a) 4 h, (b) 24 h, and (c) 72 h under ambient indoor conditions. The red dashed lines indicate the interface between substrate and inner dense layer.

Table I. Elemental composition of matrix and particles for the conversion layer with different ageing treatment. The standard deviations are based on five data points.

Element (atomic %)	0 h		4 h		24 h		72 h	
	Matrix	Particle	Matrix	Particle	Matrix	Particle	Matrix	Particle
C	5.4 ± 1.2	—	4.8 ± 2.0	10.0 ± 1.8	4.7 ± 2.4	13.9 ± 1.7	4.8 ± 2.5	11.6 ± 2.6
O	35.1 ± 5.1	—	35.1 ± 4.0	46.6 ± 3.1	33.5 ± 3.4	45.5 ± 1.1	34.9 ± 1.3	46.4 ± 1.4
Mg	1.4 ± 0.11	—	1.4 ± 0.2	1.0 ± 0.1	1.5 ± 0.1	1.1 ± 0.1	1.5 ± 0.2	0.9 ± 0.1
Al	56.7 ± 6.2	—	57.4 ± 5.0	40.9 ± 3.4	58.9 ± 4.3	38.6 ± 1.9	57.6 ± 3.1	40.1 ± 2.4
Cu	1.0 ± 0.1	—	1.4 ± 0.8	0.7 ± 0.1	1.1 ± 0.2	0.8 ± 0.1	0.9 ± 0.1	0.7 ± 0.2
Cl	0.3 ± 0.1	—	0.5 ± 0.1	0.8 ± 0.1	0.3 ± 0.1	0.2 ± 0.1	0.3 ± 0.1	0.3 ± 0.1

continuous wavelet transform has already been applied in earlier work to analyse the conversion layer growth and its irreversibility properties.[47] While the noise resistance is able to reveal the variations of the barrier properties of the conversion layers with different ageing times, the dominant types of corrosion are not reflected clearly in the time domain. For the CWT analysis presented here, four timeframes with a duration of 1000 s each are selected from the current signals in Fig. 2 at the early stages of the corrosion dominant phase, in order to exclude the influence of lithium carbonate as much as possible. Another criterium for the selection of suitable timeframes is that the system should be in a relatively stable state, i.e. the corresponding potential signals should be relatively stable. This is the case for the timeframe between 7500 s and 8500 s for the 0 h aged sample, between 4500 s and 5500 s for the 4 h aged sample, between 3500 s and 4500 s for the 24 h aged sample and between 2500 s and 3500 s for the 72 h aged sample.

In this work, the current signals are adopted because the EN current noise is able to reveal the corrosion intensity as well. Figure 10 shows the CWT spectrum of the four different timeframes. It is observed that the corrosion rate exhibits an increase and then a gradual decrease with increased ageing times, according to the maximum values of the scale bars, which corresponds well with the observations from the noise resistance. The 4 h aged sample shows the highest corrosion rate, which might be caused by the combination of a lower local concentration of lithium carbonate and the fact that the aged conversion layer does not fully develop within only 4 h. The distribution of the signal energy over time and frequency reveals the dominant electrochemical kinetics with the highest energy contribution and its evolution over time.[57]

From Fig. 10, it can be observed that the largest energy peak marked in red shifts towards lower frequencies from 0 h to 4 h and then slightly back in the high-frequency direction. A clearer view of the energy-frequency distribution is shown in the EDPs in Fig. 11. Here, the relative energy contribution of D2 and D3, D7 and D8 are added together since these represent activation-controlled and diffusion-controlled processes, respectively. A detailed relative energy distribution value is shown in Table SI. In this study, activation-controlled processes usually are attributed to fast metastable pitting and repassivation which is related to the influence of inhibition, while diffusion-control corresponds to a stable, gradually proceeding (localized corrosion) process.[57] It is observed that the 0 h aged sample possesses the largest energy contribution in D2+D3, indicating a high local concentration of lithium carbonate even though the corrosion process suppresses the inhibition function. The energy contribution of D7+D8 shows an increasing and then a decreasing trend, which is opposite to the trend of the noise resistance or corrosion intensity from the CWT spectrum. As mentioned before, the 4 h aged conversion layer contains a lower concentration of lithium carbonate, whereas the barrier properties do not improve notably. A smaller energy contribution of diffusion-controlled processes for samples with longer ageing times indicates that the longer-aged conversion layer is more able to suppress stable localized corrosion.

Entrapment of water and lithium carbonate ions.—While the residual 0.01 M NaCl solution still forms a very thin aqueous layer on the surface after initial rinsing, it is very difficult to support the continuous growth of the conversion layer for 72 h when exposed to ambient air. Water evaporation is able to remove all surface adsorbed water within several hours. Previous studies have revealed that the columnar layer and the dense inner layer both contain trapped water, especially the inner layer which is composed of amorphous lithium-incorporated aluminium hydroxides.[36,63]

To study the potential entrapment of the lithium and carbonate ions inside the conversion layer, two electrochemical cells with lower surface-to-volume ratio during the conversion formation period, generated by either increasing the volume of electrolyte or reducing the exposed surface, are adopted. Their corresponding re-immersion EN signals only show a relatively minor potential drop, as shown in Fig. 12. This implies that the amount of trapped lithium carbonate is nearly negligible in that case and this also suggests that the local alkalinity during the inhibition stage is not caused by the dissolution of the aluminium hydroxide gel. A high surface-to-volume ratio results in a sharper pH decrease during the layer growth stage, since the growth of the conversion layer consumes hydroxyl ions. A lower pH will cause a slower matrix dissolution rate and benefits the formation of the inner dense layer.[59] Thus, the inner dense layer might play an essential role in trapping mobile lithium

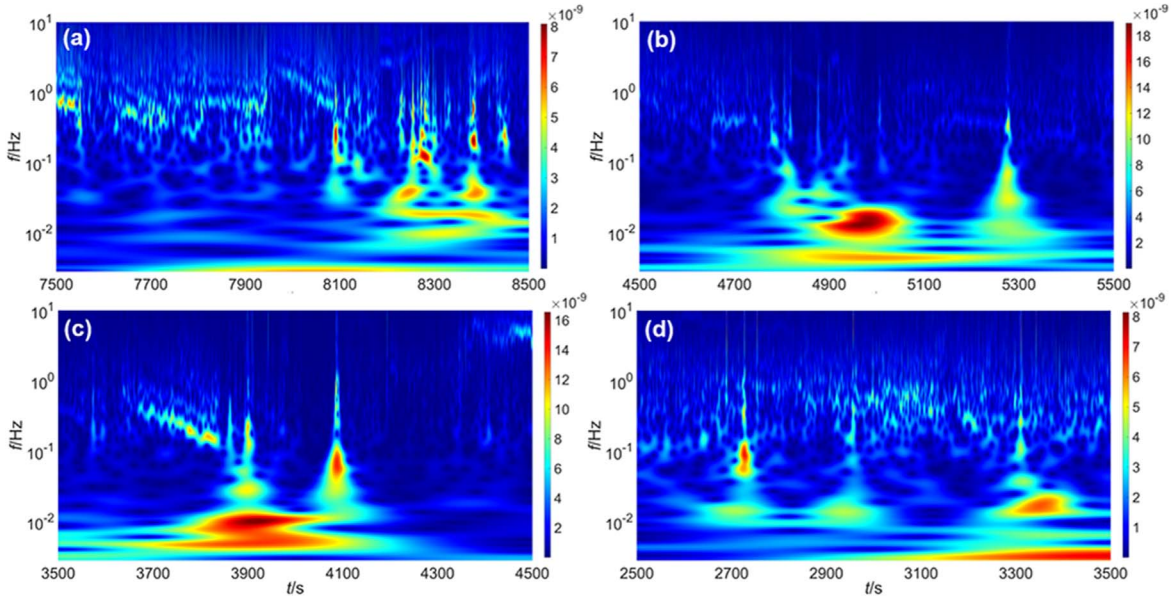

Figure 10. CWT spectrum of the EN current noise for AA2024-T3 immersed in 0.01 M NaCl and 0.01 M Li_2CO_3 solution for a duration of 14500 s (approximately 4 h) and exposed in 0.01 M NaCl solution after ageing in the air for (a) 0 h, (b) 4 h, (c) 24 h, and (d) 72 h.

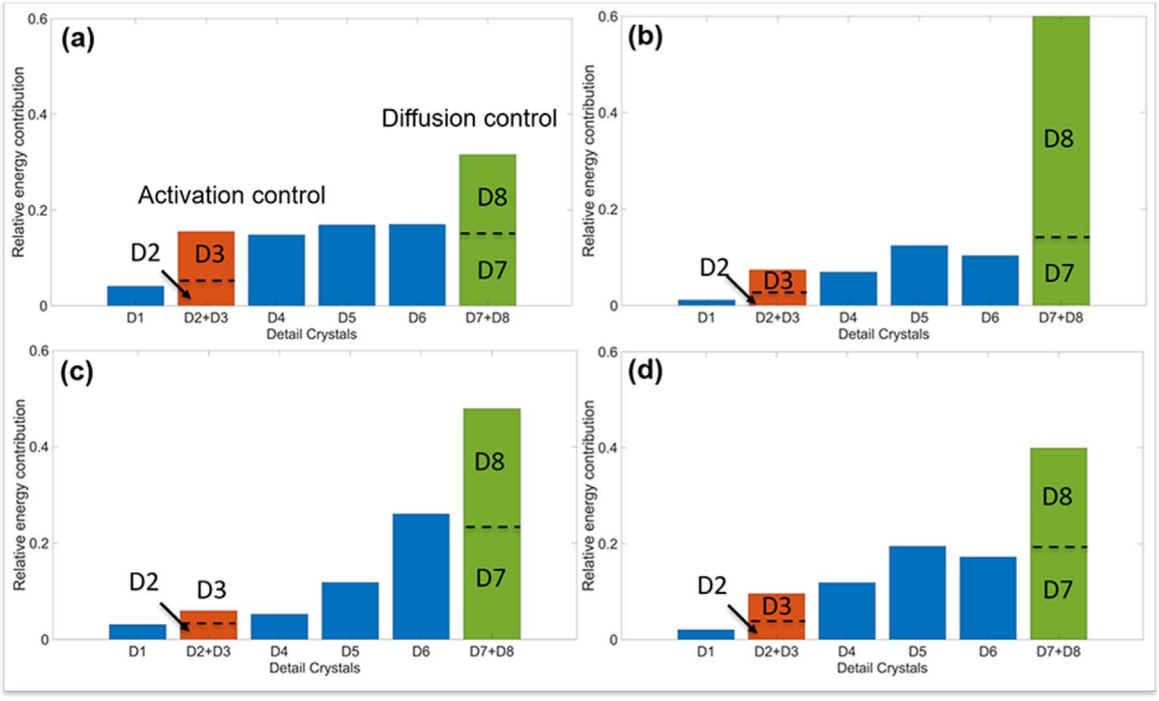

Figure 11. Energy distribution plots of the EN current signals for AA2024-T3 immersed in 0.01 M NaCl and 0.01 M Li_2CO_3 solution for 14500 s (approximately 4 h) and exposed to 0.01 M NaCl after ambient ageing for (a) 0 h, (b) 4 h, (c) 24 h and (d) 72 h. Timeframes are between (a) 7500 and 8500 s, (b) 4500 and 5500 s, (c) 3500 and 3500 s and (d) 2500 and 3500 s.

carbonate, but the detailed mechanism still requires further investigation.

Morphological evolution model.—Based on the results and discussion above, it is inferred that the appearance of particles on the conversion layer is due to the heterogeneous growth of the conversion layer. A schematic overall morphological evolution model is depicted in Fig. 13. A thin electrolyte layer remains on the conversion layer surface after the removal of the original lithium-containing solution. Although the surface has been gently rinsed by 0.01 M NaCl solution, the conversion layer still traps some mobile ions like lithium, carbonate and aluminate, as well as water molecules. At a later stage, the continuous thin water layer gradually discretizes to local regions due to water evaporation. The continuous growth of the conversion layer only occurs where water still exists and lithium, carbonate, aluminate ions and water will be gradually consumed locally. It has been reported before that the formation of the columnar structure is promoted by local environments exhibiting a relatively higher pH and lithium ion concentration.[32] The highly limited aqueous volume generates a higher concentration of lithium ions and the carbonate generates a higher pH. The ultra-thin water layer also enables the supply of oxygen, which in turn plays a critical

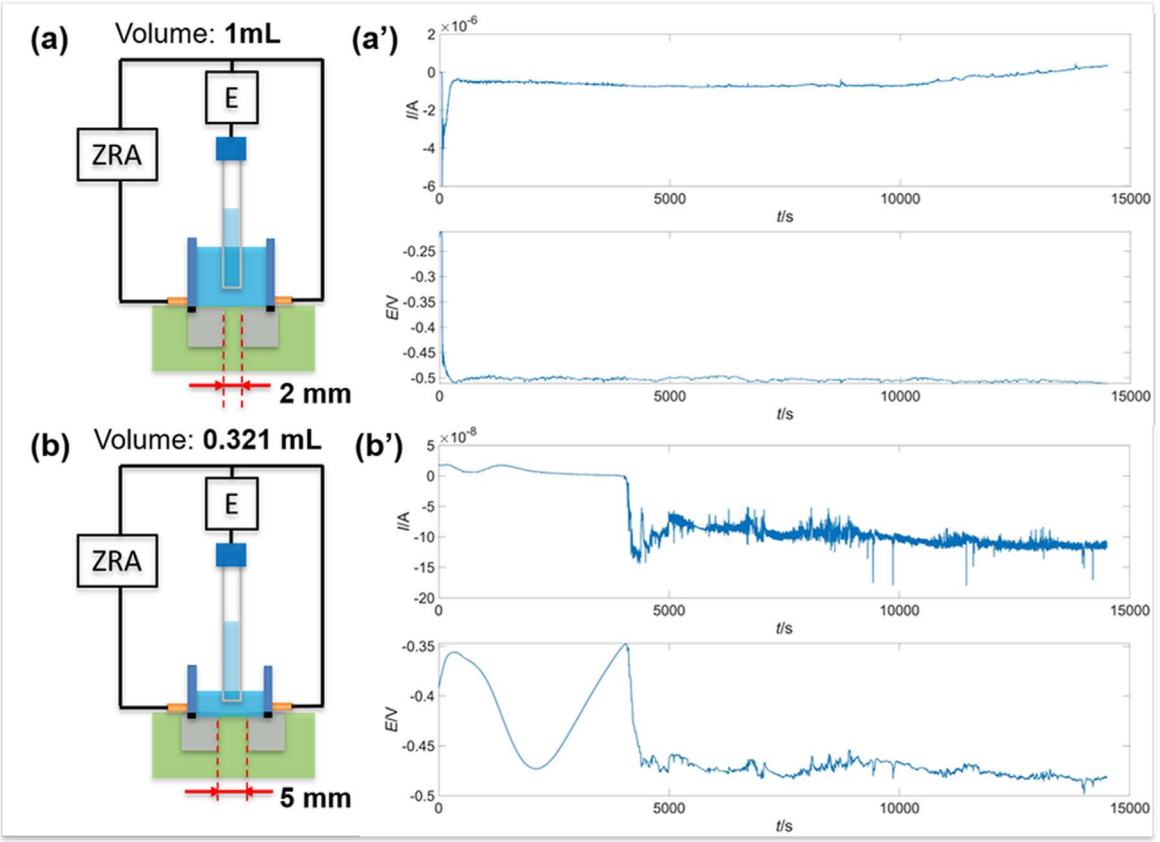

Figure 12. Electrochemical cell set-up of immersion treatment with different surface area-to-volume ratios and corresponding re-immersion EN current and potential signals in 0.01 M NaCl solution for 14500 s (approximately 4 h).

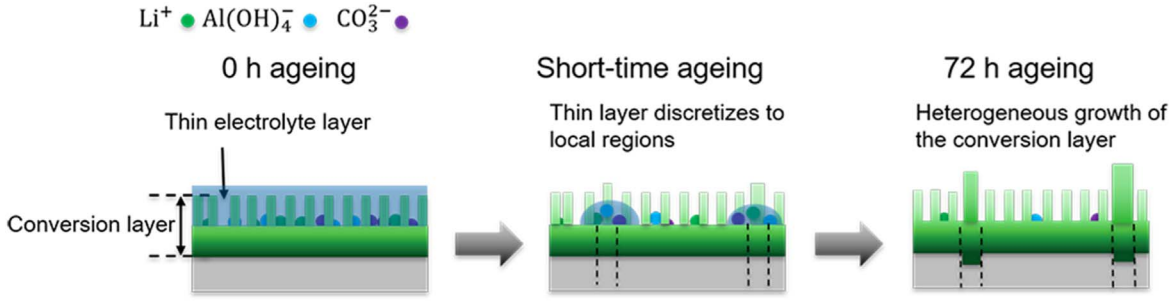

Figure 13. Schematic of morphological evolution during the ageing treatment.

role in the formation of the Li-Al layered double hydroxide (LDH) structure.[24,28] This explains why the particles exhibit a porous structure and why the oxygen and carbon contents are higher than those at uniform conversion layer surface areas. In addition, the high local pH also promotes corrosion of the aluminium matrix underneath the water layer, forming a thicker inner dense layer at the location of the particles. Although the continuous growth of the conversion layer is mainly heterogeneous during ageing, the bare regions of the conversion layer may still develop to a small extent, resulting in slightly improved barrier properties. In addition, the influence of intermetallic particles on the continuous growth of the conversion layer still remains unclear, which requires further study in the future.

Time-dependent morphological and compositional variations of the conversion layer led to distinct EN signals as shown in Fig. 2. Based on the general model as proposed in Figs. 13, 14 further explains the differences in time-dependent behaviour of the conversion layers with four different ageing treatments during re-immersion. For the 0 h aged conversion layer, the trapped lithium carbonate leaches from the conversion layer immediately at the beginning of re-immersion, leading to a local pH increase. Although the local environment becomes more aggressive, the presence of lithium and carbonate ion provide the growth conditions of the lithium-based conversion layer. The large oscillations observed in the noise resistance (Figs. 3a and 3b) indicate the competitive dissolution and growth of the conversion layer.[48] The local concentration of lithium and carbonate ions continues to decrease during re-immersion and the inhibition stage terminates when the local concentration becomes lower than the minimum amount that is required for effective protection. The appearance of superimposed transient signals indicates that localised corrosion is dominant. For samples with longer ageing treatments, the concentration of available lithium carbonate is lower at the beginning due to the consumption of lithium carbonate by the continuous growth of the conversion layers during ageing. Therefore, the dominant corrosion stage initiates earlier in these cases as compared to samples with

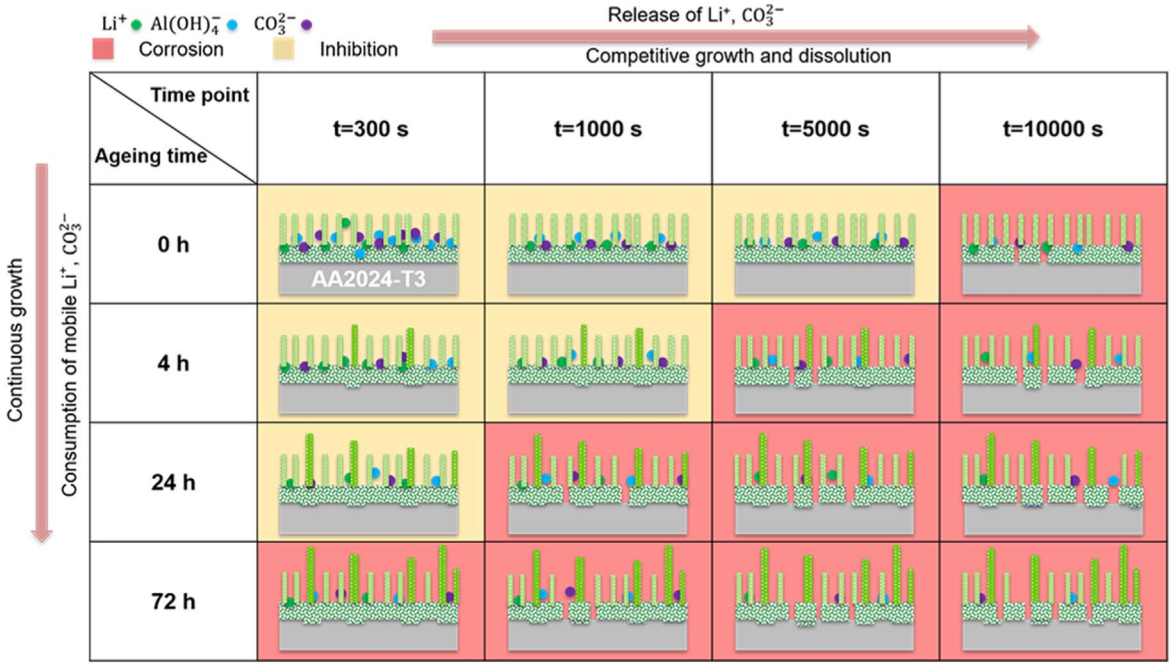

Figure 14. Schematic representation of the compositional and morphological evolution of the conversion layer during re-immersion for different preceding ambient ageing times.

shorter ageing times. For samples with 72 h ageing treatment, the initial concentration of mobile lithium carbonate is lower than the minimum demand for inhibition. Therefore, inhibition does not occur during the re-immersion period for the samples with long ageing times.

Conclusions

In this work, the influence of an ambient ageing treatment on the protective behaviour of lithium-based conversion layers is studied. Ageing for different durations up to 72 h under ambient indoor conditions causes a distinct difference in corrosion protective properties of these conversion layers. The freshly-formed lithium-based layer traps water and lithium carbonate. This trapped mobile lithium carbonate will be incorporated into the conversion layer gradually and locally during ageing, leading to a heterogenous growth of the conversion layer. The fresh conversion layer is able to temporarily maintain an inhibited state with high corrosion resistance and shows active inhibition through leaching of entrapped lithium carbonate during the first stage of the re-immersion tests. At a later stage, the conversion layer shows a much lower resistance after the depletion of leachable lithium carbonate as compared to the longer-aged conversion layers. Long-time ageing treatment significantly decreases the initial active protection ability but improves the overall corrosion barrier resistance of the conversion layer, as a result of the ongoing development of the conversion layer during ageing.

Credit Authorship Contribution Statement

Ziyu Li designed the research project, performed the experiments, analysed the data, and finalized the original draft. Mohammad Soleimani contributed to FIB/SEM characterization. Peter Visser reviewed the manuscript and contributed to the discussion. Axel Homborg, Yaiza Gonzalez-Garcia, and Arjan Mol supervised the experiments, reviewed the manuscript, and contributed to the discussion.

Acknowledgments

The authors wish to acknowledge the financial support from the China Scholarship Council (CSC). The authors also acknowledge the helpful scientific discussion with Dr. Ali Kosari.

Competing Interests

The authors declare no competing interests.

Data Availability

Data will be made available on request.

ORCID

Ziyu Li https://orcid.org/0000-0002-5402-8071
Peter Visser https://orcid.org/0000-0002-6388-382X
Arjan Mol https://orcid.org/0000-0003-1810-5145

References

1. N. L. Sukiman, X. Zhou, N. Birbilis, A. E. Hughes, J. M. C. Mol, S. J. Garcia, X. Zhou, G. E. Thompson, and Z. Ahmad, *Aluminium Alloys - New Trends in Fabrication and Applications* (Rijeka, InTech) Vol. 47 (2012).
2. A. E. Hughes, N. Birbilis, J. M. C. Mol, S. J. Garcia, X. Zhou, G. E. Thompson, and Z. Ahmad, *Recent Trends in Processing and Degradation of Aluminium Alloys* (Rijeka, InTech)p. 223 (2011).
3. A. E. Hughes, C. MacRae, N. Wilson, A. Torpy, T. H. Muster, and A. M. Glenn, *Surf. Interface Anal.*, **42**, 334 (2010).
4. A. Boag, A. E. Hughes, N. C. Wilson, A. Torpy, C. M. MacRae, A. M. Glenn, and T. H. Muster, *Corros. Sci.*, **51**, 1565 (2009).
5. A. Boag, A. E. Hughes, A. M. Glenn, T. H. Muster, and D. McCulloch, *Corros. Sci.*, **53**, 17 (2011).
6. N. Birbilis, Y. M. Zhu, S. K. Kairy, M. A. Glenn, J. F. Nie, A. J. Morton, Y. Gonzalez-Garcia, H. Terryn, J. M. C. Mol, and A. E. Hughes, *Corros. Sci.*, **113**, 160 (2016).
7. A. Kosari, F. Tichelaar, P. Visser, H. Zandbergen, H. Terryn, and J. M. C. Mol, *Corros. Sci.*, **177**, 108947 (2020).
8. M. Becker, *Corros. Rev.*, **37**, 321 (2019).
9. H. R. Fischer, S. J. García, and R. G. Buchheit, *Active Protective Coatings: New-Generation Coatings for Metals* (Berlin)(Springer)p. 139 (2016).
10. P. Visser, H. Terryn, J. M. C. Mol, A. E. Hughes, J. M. C. Mol, M. L. Zheludkevich, and R. G. Buchheit, "Active Protective Coatings: New-Generation Coatings for Metals." *Springer Series in Materials Science* (Berlin)(Springer)p. 315 (2016).
11. H. Costenaro, A. Lanzutti, Y. Paint, L. Fedrizzi, M. Terada, H. G. de Melo, and M. G. Olivier, *Surf. Coat. Technol.*, **324**, 438 (2017).

12. M. Saenz de Miera, M. Curioni, P. Skeldon, and G. E. Thompson, *Corros. Sci.*, **52**, 2489 (2010).
13. M. Paz Martinez-Viademonte, S. T. Abrahami, M. D. Havigh, K. Marcoen, T. Hack, M. Burchardt, and H. Terryn, *Coatings*, **12**, 908 (2022).
14. N. N. Voevodin, J. W. Kurdziel, and R. Mantz, *Surf. Coat. Technol.*, **201**, 1080 (2006).
15. A. Conde, A. Durán, and J. J. de Damborenea, *Prog. Org. Coat.*, **46**, 288 (2003).
16. A. Trentin, S. V. Harb, M. C. Uvida, S. H. Pulcinelli, C. V. Santilli, K. Marcoen, S. Pletincx, H. Terryn, T. Hauffman, and P. Hammer, *ACS Appl. Mater. Interfaces*, **11**, 40629 (2019).
17. M. Becker, *Corros. Rev.*, **37**, 321 (2019).
18. P. Santa Coloma, U. Izagirre, Y. Belaustegi, J. B. Jorcin, F. J. Cano, and N. Lapeña, *Appl. Surf. Sci.*, **345**, 24 (2015).
19. I. Milošev and G. S. Frankel, *J. Electrochem. Soc.*, **165**, C127 (2018).
20. J. K. Hawkins, H. S. Isaacs, S. M. Heald, J. Tranquada, G. E. Thompson, and G. C. Wood, *Corros. Sci.*, **27**, 391 (1987).
21. A. E. Hughes, R. J. Taylor, and B. R. W. Hinton, *Surf. Interface Anal.*, **25**, 223 (1997).
22. O. Gharbi, S. Thomas, C. Smith, and N. Birbilis, *Npj Mater. Degrad.*, **2**, 12 (2018).
23. J. Gui and T. M. Devine, *Scr Met. U. S.*, **21**, 6 (1987).
24. C. M. Rangel and M. A. Travassos, *Corros. Sci.*, **33**, 327 (1992).
25. G. R. Williams and D. O'Hare, *J. Phys. Chem. B*, **110**, 10619 (2006).
26. C. M. Rangel and M. A. Travassos, *Surf. Coat. Technol.*, **200**, 5823 (2006).
27. R. G. Buchheit, M. D. Bode, and G. E. Stoner, *Corrosion*, **50**, 205 (1994).
28. C. A. Drewien, M. O. Eatough, D. R. Tallant, C. R. Hills, and R. G. Buchheit, *J. Mater. Res.*, **11**, 1507 (1996).
29. M. W. Kendig and R. G. Buchheit, *Corrosion*, **59**, 379 (2003).
30. P. Visser and S. A. Hayes, "Anti-corrosive coating composition." *WIP Organization (Ed.), WO*, **112605**, A1 (2010).
31. P. Visser, Y. Liu, H. Terryn, and J. M. C. Mol, *J. Coat. Technol. Res.*, **13**, 557 (2016).
32. Y. Liu, P. Visser, X. Zhou, S. B. Lyon, T. Hashimoto, M. Curioni, A. Gholinia, G. E. Thompson, G. Smyth, and S. R. Gibbon, *J. Electrochem. Soc.*, **163**, C45 (2015).
33. Y. Liu et al., *Surf. Interface Anal.*, **48**, 798 (2016).
34. P. Visser, A. Lutz, J. M. C. Mol, and H. Terryn, *Prog. Org. Coat.*, **99**, 80 (2016).
35. P. Visser, H. Terryn, and J. M. C. Mol, *Corros. Sci.*, **140**, 272 (2018).
36. A. Kosari, P. Visser, F. Tichelaar, S. Eswara, J.-N. Audinot, T. Wirtz, H. Zandbergen, H. Terryn, and J. M. C. Mol, *Appl. Surf. Sci.*, **512**, 145665 (2020).
37. A. Kosari, F. Tichelaar, P. Visser, H. Zandbergen, H. Terryn, and J. M. C. Mol, *Corros. Sci.*, **190**, 109651 (2021).
38. P. Visser, K. Marcoen, G. F. Trindade, M.-L. Abel, J. F. Watts, T. Hauffman, J. M. C. Mol, and H. Terryn, *Corros. Sci.*, **150**, 194 (2019).
39. P. Visser, H. Terryn, and J. M. C. Mol, *Surf. Interface Anal.*, **51**, 1276 (2019).
40. L. Li and G. M. Swain, *ACS Appl. Mater. Interfaces*, **5**, 7923 (2013).
41. P. Zhou, B. Yu, Y. Hou, G. Duan, L. Yang, B. Zhang, T. Zhang, and F. Wang, *Corros. Sci.*, **178**, 109069 (2021).
42. V. Laget, C. S. Jeffcoate, H. S. Isaacs, and R. G. Buchheit, *J. Electrochem. Soc.*, **150**, B425 (2003).
43. Y. Guo and G. S. Frankel, *Surf. Coat. Technol.*, **206**, 3895 (2012).
44. X. Liu, M. Wang, H. Li, L. Wang, and Y. Xu, *Corros. Sci.*, **167**, 108538 (2020).
45. M. A. Kamde, Y. Mahton, J. Ohodnicki, M. Roy, and P. Saha, *Surf. Coat. Technol.*, **421**, 127451 (2021).
46. M. Yuan, J. Lu, G. Kong, and C. Che, *Surf. Coat. Technol.*, **205**, 4466 (2011).
47. Z. Li, A. Homborg, Y. Gonzalez-Garcia, A. Kosari, P. Visser, and A. Mol, *Electrochim. Acta*, **426**, 140733 (2022).
48. P. Visser, Y. Gonzalez-Garcia, J. M. C. Mol, and H. Terryn, *J. Electrochem. Soc.*, **165**, C60 (2018).
49. D.-H. Xia and Y. Behnamian, *Russ. J. Electrochem.*, **51**, 593 (2015).
50. F. Mansfeld, Z. Sun, and C. H. Hsu, *Electrochim. Acta*, **46**, 3651 (2001).
51. F. Mansfeld and Z. Sun, *Corrosion*, **55**, 915 (1999).
52. A. M. Homborg, T. Tinga, X. Zhang, E. P. M. van Westing, P. J. Oonincx, J. H. W. de Wit, and J. M. C. Mol, *Electrochim. Acta*, **70**, 199 (2012).
53. D.-H. Xia, S. Song, Y. Behnamian, W. Hu, Y. F. Cheng, J. Luo, and F. Huet, *J. Electrochem. Soc.*, **167**, 081507 (2020).
54. R. A. Cottis, *Corrosion*, **57**, 265 (2001).
55. H. Ashassi-Sorkhabi, D. Seifzadeh, and M. G. Hosseini, *Corros. Sci.*, **50**, 3363 (2008).
56. A. M. Homborg, T. Tinga, E. P. M. van Westing, X. Zhang, G. M. Ferrari, J. H. W. de Wit, and J. M. C. Mol, *Corrosion*, **70**, 971 (2014).
57. S. S. Jamali, *Prog. Org. Coat.*, **95**, 26 (2016).
58. P. Visser, M. Meeusen, Y. Gonzalez-Garcia, H. Terryn, and J. M. C. Mol, *J. Electrochem. Soc.*, **164**, C396 (2017).
59. A. Kosari, F. Tichelaar, P. Visser, P. Taheri, H. Zandbergen, H. Terryn, and J. M. C. Mol, *Npj Mater. Degrad.*, **5**, 40 (2021).
60. A. Kosari, H. Zandbergen, F. Tichelaar, P. Visser, P. Taheri, H. Terryn, and J. M. C. Mol, *Corros. Sci.*, **177**, 108912 (2020).
61. A. Kosari, M. Ahmadi, F. Tichelaar, P. Visser, Y. Gonzalez-Garcia, H. Zandbergen, H. Terryn, and J. M. C. Mol, *J. Electrochem. Soc.*, **168**, 041505 (2021).
62. K. Marcoen, P. Visser, G. F. Trindade, M.-L. Abel, J. F. Watts, J. M. C. Mol, H. Terryn, and T. Hauffman, *Prog. Org. Coat.*, **119**, 65 (2018).
63. B. R. Baker and R. M. Pearson, *J. Catal.*, **33**, 265 (1974).